Fracture Mechanics of Concrete and Concrete Structures -
Assessment, Durability, Monitoring and Retrofitting of Concrete Structures- B. H. Oh, et al. (eds)

Monitoring corrosion-induced cracks in concrete by acoustic emission

Y. Tomoda
Faculty of Engineering, Kumamoto University, Kurokami, Kumamoto, Japan

K. Mori
Taiheiyou Cement Corporation, Sakura, Tiba, Japan

Y. Kawasaki & M. Ohtsu
Graduate School of Science and Technology, Kumamoto University, Kurokami, Kumamoto, JAPAN

ABSTRACT: Concrete structures suffer from the corrosion of reinforcing steel-bars due to severe environments, in particular, chloride attack. Acoustic Emission (AE) techniques have been extensively applied to concrete and concrete structures. In order to identify the onset of corrosion and the nucleation of concrete cracking due to expansion of corrosion products, continuous AE monitoring is available. These corrosion-induced cracks in concrete are studied in an accelerated corrosion test, where kinematics of micro-cracks is identified by SiGMA (**Si**mplified **G**reen's functions for **M**oment tensor **A**nalysis). Monitoring the corrosion process of rebar by AE, it is confirmed that the onset of corrosion and the nucleation of corrosion-induced cracks in concrete are successfully identified. Then, generating mechanisms of corrosion-induced cracks are clarified by the SiGMA analysis.

1 INTRODUCTION

In order to avoid harmful corrosion damages before reaching critical level, a variety of monitoring methods have been developed (Dubravka et al., 2000). One effective method is nondestructive evaluation (NDE), by which the corrosion of rebar is evaluated quickly and inexpensively, using a sensor or a probe placed on the surface of existing concrete structures, or embedded inside concrete for new structures. NDE methods are practical and useful in both a laboratory test and on-site measurement. So far, electrochemical techniques of the half-cell potential, the polarization resistance and so forth are widely employed. The corrosion potentials or currents during the electrochemical corrosion process are evaluated. Recently, acoustic emission (AE) (Ohtsu, 2003) method is introduced for detecting micro-cracks generated by corrosion.

According to the relationship between deterioration of RC structures and a lifecycle of RC structure shown in Figure 1 (JSCE, 2001), deterioration process of a concrete structure due to corrosion is divided into four stages of dormant, initiation, acceleration and deterioration. Since the dormant stage is governed by penetration of chloride ions, onset of corrosion depends on the microstructure of concrete, the external environment and initial concentration of chloride ions, the thickness of cover and so on. When the chloride concentration at the rebar surface

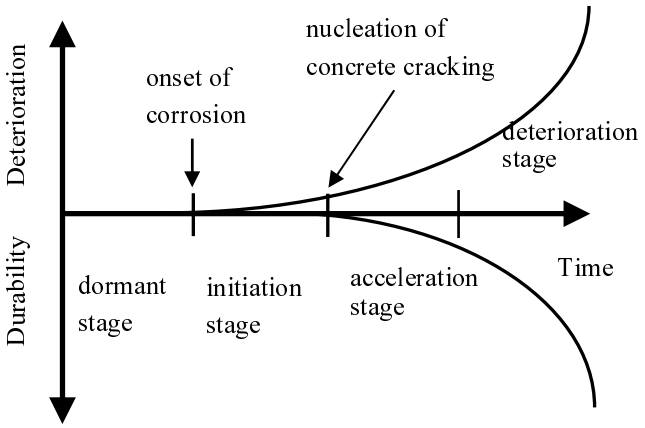

Figure 1. Deterioration process due to corrosion.

exceeds the critical value, a passive film on the surface of rebar is destroyed. Then the onset of corrosion is started. Following the stage, the electrochemical reaction is initiated and continues with supplying oxygen and water. Then, corrosion products on surfaces of rebar grow with time and nucleate micro cracks in concrete. This corresponds to the initiation stage in Figure 1. NDE methods are applied to detect the corrosion at an early stage. Normally, the electrochemical techniques are applicable after the initiation stage. It is reported (Ohtsu, 2003, Ohtsu & Tomoda, 2008) that the onset of corrosion and the nucleation of concrete cracking are qualified from AE activity. Consequently, continuous AE

measurement is applied to identify the transition periods at the onset of corrosion and at the nucleation cracking. Comparing with diffusion analysis of chloride ions, AE activities are investigated in experiments and result are confirmed by scanning electron micrograph (SEM).

The identification of fracture process zone by strain gages and displacement transducers are limited, whereas AE techniques are able to estimate these zones by taking into account AE source cluster. As for the progress of micro-cracks in concrete, SiGMA (Simplified Green's functions for Moment tensor Analysis) procedure has been successfully applied (Ohtsu 1991 Ohtsu & Shigeishi, Ohno et al. 2008). Such kinematics of an AE source, as crack location, crack type and crack orientation are identified by AE parameter and SiGMA analysis from detected AE waveforms.

2 AE PARAMETER ANALYSIS

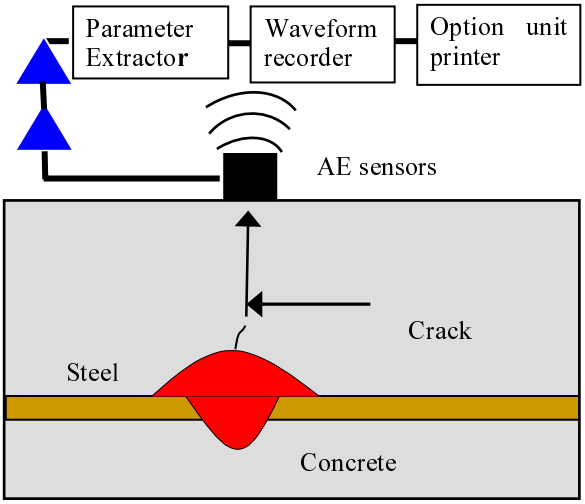

Figure 2. AE measurement.

AE is detected by micro-cracking due to the corrosion as shown in Figure 2 (Ohtsu, 1996). AE events are associated with cracking and are detected by AE sensors as electrical signals, which are amplified, filtered, and processed. An AE signal is characterized by employing AE parameters such as energy, counts, event, amplitude, rise time and duration as illustrated in Figure 3. Characteristics of AE signals are estimated by using two indices of RA value and average frequency, which are defined from wave parameters as,

$$\text{RA} = \text{Rise time/Amplitude} \quad (1)$$

$$\text{Average Frequency} = \text{Counts/Duration} \quad (2)$$

According to the JCMS-III B5706 standard (JCMS-III, 2003), a crack type is classified from the relationship between RA value and the average frequency, which is given in Figure 4. A tensile-type

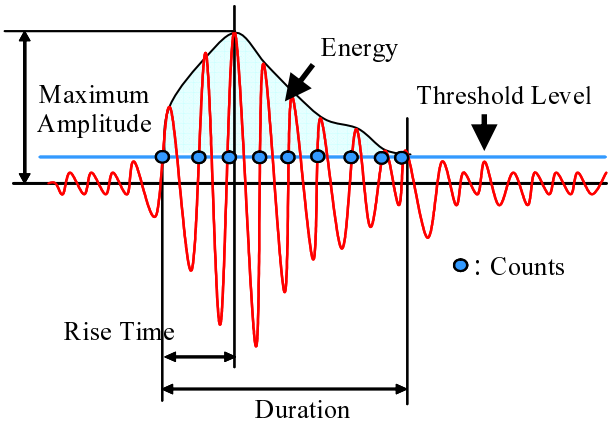

Figure 3. AE signal parameters.

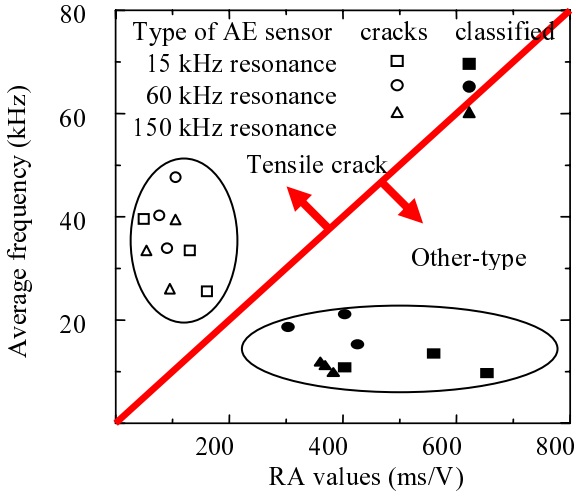

Figure 4. Classification of cracks by AE indices.

crack is referred to as AE signal with high average frequency and low RA value. In the other way, an other-type crack than a tensile-type crack is identified.

3 THEORY OF SIGMA ANALYSIS

Since AE signals are generated due to micro-cracks, detected AE waveforms correspond to the micro-fracture in a material. Therefore, AE waveforms analysis is carried out to obtain kinematics of AE source (Grosse et al., 1997, Katsage & Young, 2007). One powerful waveform analysis is SiGMA

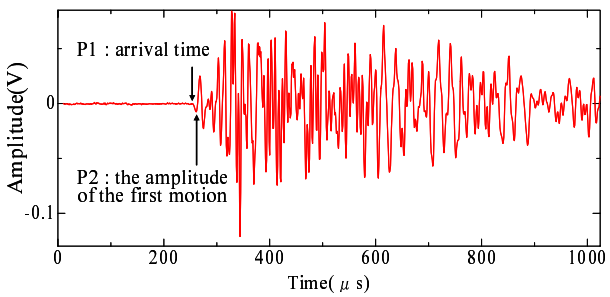

Figure 5. Detected AE waveform.

procedure. The SiGMA analysis consists of AE source location procedure and the moment tensor analysis of AE source. In the SiGMA analysis, two parameters of the arrival time (P1) and the amplitude of the first motion (P2) shown in Figure 5 are applied to the analysis. These two parameters are determined by automated detection method (Ohno et al., 2008).

AE source location $\boldsymbol{y}$ is determined from the arrival time differences $\boldsymbol{t_i}$ between the observation point $\boldsymbol{x_i}$ and $\boldsymbol{x_{i+1}}$, solving equations,

$$R_i - R_{i+1} = |x_i - y| - |x_{i+1} - y| = v_p t_i \tag{3}$$

Here, R is the distance between the source $\boldsymbol{y}$ and the observation point $\boldsymbol{x}$. $\boldsymbol{v_p}$ is the velocity of P-wave.

After determining the location of AE source, the amplitude of the first motion (P2) are substituted into following equation based on the generalized theory of AE (Ohtsu and Ono, 1984).

$$A(x) = C_S \frac{\mathrm{Ref}(t,\gamma)}{R} \cdot \gamma_p \gamma_q M_{pq} DA \tag{4}$$

Here, A ($\boldsymbol{x}$) is the amplitude of the first motion. C_S is the calibration coefficient of the sensor sensitivity and material constants. The reflection coefficient Ref ($\boldsymbol{t}$, $\boldsymbol{\gamma}$) is obtained as $\boldsymbol{t}$ is the direction of sensor sensitivity. DA is area of crack surface, M_{pq} is the moment tensor and $\boldsymbol{\gamma}$ is the direction vector of distance R from source to observation point $\boldsymbol{x}$ as shown in Figure 6.

The moment tensor M_{pq} consists of the crack-motion vector $\boldsymbol{l}$ and unit normal vector $\boldsymbol{n}$ on crack surface. In an isotropic material, the moment tensor is represented as,

$$M_{pq} = (\lambda l_k n_k \delta_{pq} + \mu l_p n_q + \mu l_q n_p)\Delta V \tag{5}$$

where $\boldsymbol{\lambda}$ and $\boldsymbol{\mu}$ are Lame constants.

Although concrete is microscopically heterogeneous material, in the case that the wave-lengths are larger than the sizes of aggregates, the effect of heterogeneous becomes minor (Ohtsu et al., 1998). Since the velocity of P-wave in concrete is about 4000 m/s, the wave-length becomes around 40 mm at 100 kHz. It results in the fact that concrete consisting of normal aggregate is reasonably referred to as isotropically homogeneous. In an isotropic material, as the moment tensor is symmetric and of the second order, the number of independent unknown components is six. Eventually, multi-channel observation of the first motions at more than six channels provides sufficient information to solve Equation 4 and to determine all moment tensor components. Since the SiGMA procedure requires only relative values of moment tensor components, the calibration by the relative coefficients is sufficient enough.

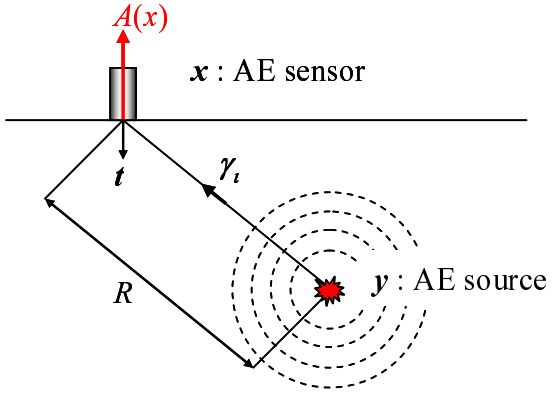

Figure 6. Crack nucleation and AE detection.

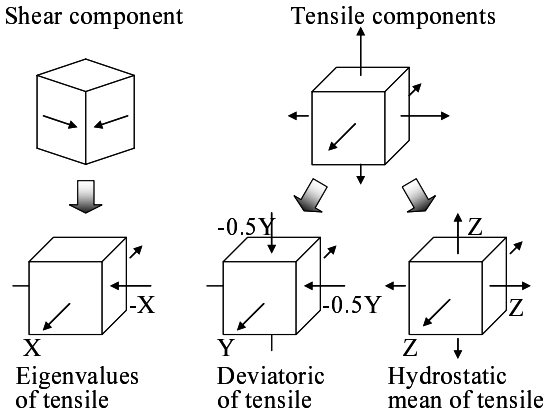

Figure 7. Unified decomposition of eigenvalues of the moment tensor.

To classify crack type, the eigenvalue analysis of the moment tensor was developed (Ohtsu, 1981). The eigenvalues of the moment tensor for a general case are represented by the combination of the shear crack and the tensile crack as shown in Figure 7. From Figure 7, the relative ratios X, Y and Z are obtained as,

$$1.0 = X + Y + Z,$$

$$\frac{\text{the intermediate eigenvalue}}{\text{the maximum eigenvalue}} = 0 - Y/2 + Z,$$

$$\frac{\text{the minimum eigenvalue}}{\text{the maximum eigenvalue}} = -X - Y/2 + Z. \tag{6}$$

In the present code, AE sources of which the shear ratios X are smaller than 40 % are classified as tensile cracks. AE sources of shear ratios X are greater than 60 % are referred to as shear cracks. In the case of the ratios between 40 % and 60 %, AE sources are classified as mixed-mode cracks. In the eigenvalue analysis, three eigenvectors $\boldsymbol{e_1}$, $\boldsymbol{e_2}$ and $\boldsymbol{e_3}$,

$$\begin{aligned} \boldsymbol{e_1} &= \boldsymbol{l} + \boldsymbol{n} \\ \boldsymbol{e_2} &= \boldsymbol{l} \times \boldsymbol{n} \\ \boldsymbol{e_3} &= \boldsymbol{l} - \boldsymbol{n}, \end{aligned} \tag{7}$$

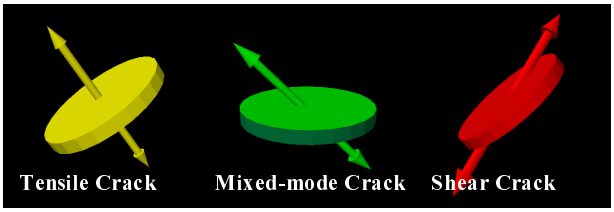

Figure 8. 3-D display models for tensile, mixed-mode and shear cracks.

are also determined. Vector l and n, which are interchangeable, are recovered. In order to visualize these kinematical information of AE sources, the Light Wave 3D software (New Tek) is introduced. Crack modes of tensile, mixed-mode and shear are given in Figure 8. Here, an arrow vector indicates a crack motion vector ***l***, and a circular plate corresponds to a crack surface which is perpendicular to a crack normal vector ***n***.

4 EXPERIMENTAL PROCEDURE

Table 1. Mix proportion and properties of concrete.

Weight per unit volume (kg/m^3)				
W/C (%)	Water	Cement	Fine aggregate	Coarse aggregate
55	180	327	704	1170
Slump	Air (%)	Maximum gravel size (mm)		
4.5	6.5	20		

RC slabs of dimensions 100 × 100 × 400 mm were made. Configuration of specimen is illustrated in Figure 9. Rebars of 13 mm diameter were embedded with 45mm cover-thicknesses for longitudinal arrangement. Mixture proportion of concrete is given in Table 1. Following the standard curing for 28

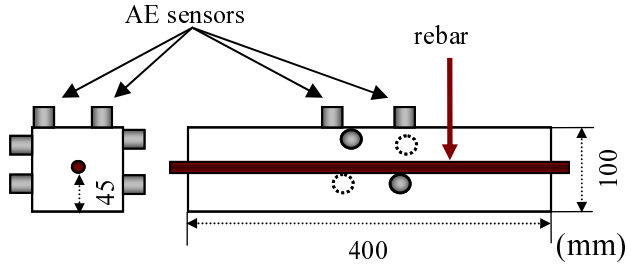

Figure 9. Sketch of Reinforced concrete slab tested.

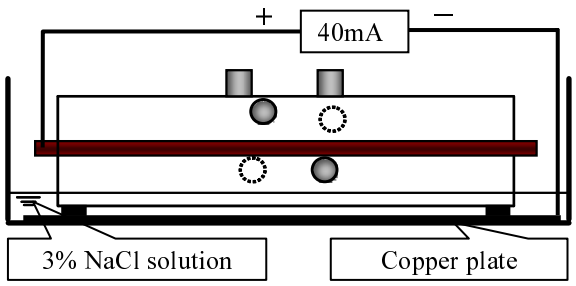

Figure 10. Test set up for accelerated corrosion test.

days in 20°C water, all surfaces of the specimen were coated by epoxy, except the bottom surface for one-dimensional diffusion.

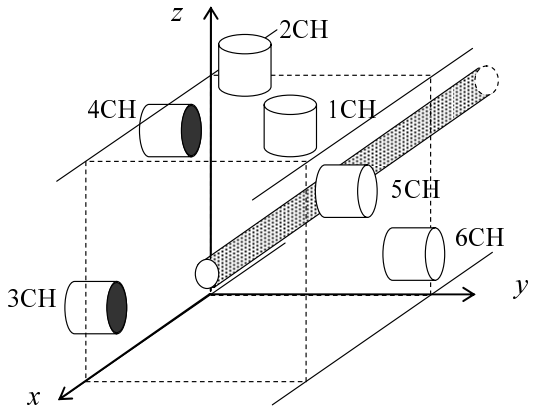

Figure 11. Set of AE sensors.

In an accelerated corrosion test, the specimen was placed on a copper plate in a container filled with 3% NaCl solution as shown in Figure 10. Between rebar and the copper plate, 40mA electric current was continuously charged.

Table 2. Coordinates of AE sensors.

	x(m)	Y(m)	z(m)
1CH	0.090	0.090	0.100
2CH	0.010	0.030	0.100
3CH	0.085	0.000	0.033
4CH	0.030	0.000	0.085
5CH	0.090	0.100	0.075
6CH	0.020	0.100	0.033

AE measurement was continuously conducted by using Disp (PAC), during the corrosion process along with the electrochemical measurements. Six AE sensors were attached as shown in Figure 11 and coordinates of AE sensors given in Table 2. AE sensors of type R-15 (150 kHz resonance) were used. Frequency range of the measurement was 10 kHz ~ 2MHz and total gain was 60 dB. The threshold level was set to 40 dB. Every day, AE measurement was temporarily stopped for the electrochemical measurement.

Half-cell potentials at the surface of the specimen were measured by a portable corrosion meter, SRI-CM-II (Yokota al., 1999). Potentials were measured at three locations on the bottom surface of the specimen. The specimen was measured every day until the average potential reached to -350mV (CSE). Then results of the half-cell potentials were converted to the probability of corrosion by ASTM C876 standard (ASTM, 1991), which is prescribed in Table 3.

Table 3. Criterion for half-cell potential (mV, CSE).

Potential	Corrosion probability
-200mV < E	90% no corrosion
-350mV < E ≤ -200mV	Uncertain
E < -350mV	90% corrosion

5 RESULTS AND DISCUSSION

5.1 *AE activity in the accelerated corrosion test*

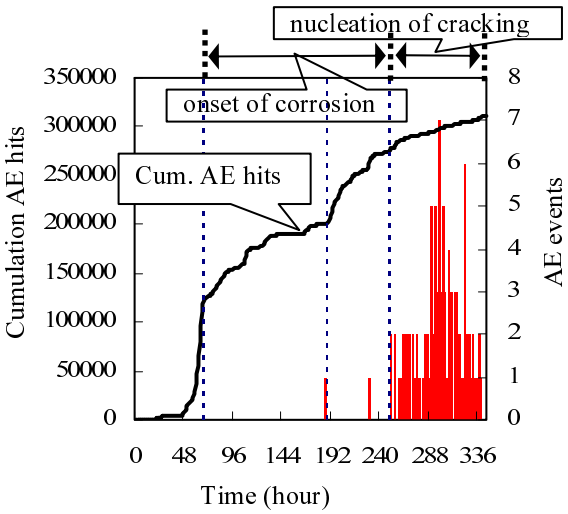

Figure 12. Cumulation AE hits and AE events.

Cumulative AE hits and AE events for all 6 channels are shown in Figure 12. An AE event is the phenomenon which one AE hit was measured by out of five sensors from among six sensors. AE hits start to increase at the period from 47 hours to 92 hours. From 189 hours elapsed to 214 hours, another AE activity is observed. After 229 hours elapsed, a very active period of AE generation is found. Then, at 324 hours elapsed, the test was terminated and cracks and rust stain were observed as seen in Figure 13. Comparing the curve of cumulative AE hits with that of deterioration process due to corrosion in Figure 1 corresponds to the initiation stage and the acceleration stage. Thus, onset of corrosion and nucleation of concrete cracking of AE activity are assigned in Figure 12.

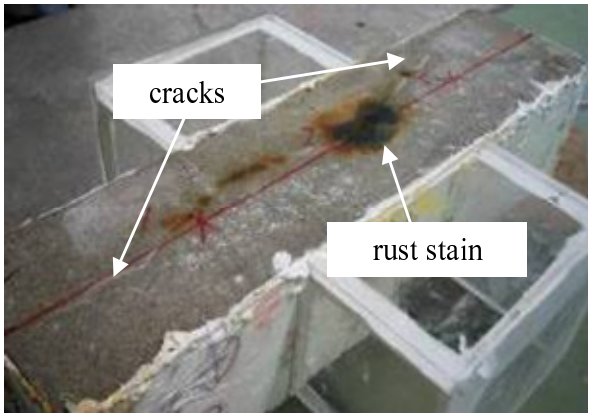

Figure 13. End test specimen of a test.

5.2 *AE activity and Half-cell potentials*

Cumulative AE hits are compared with half-cell potentials in Figure 14. Although the half-cell potentials started as positive values, they reasonably decrease at the 1st period. Then, potentials gradually

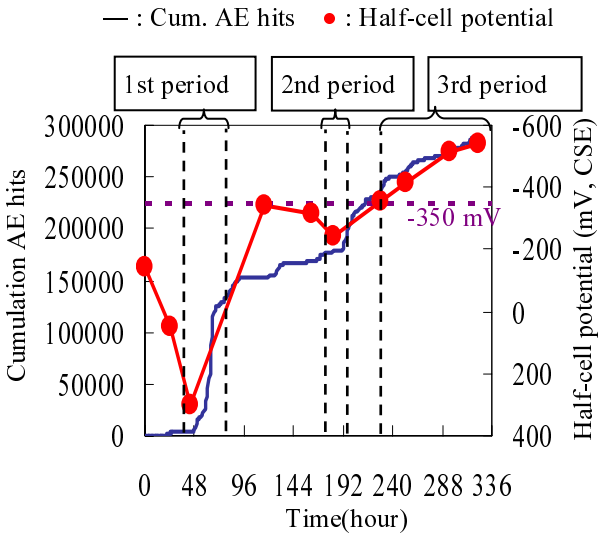

Figure 14. Cumulation AE hits and Half-cell potentials.

increase at the 2nd phase in Figure 1 and begin to decrease at the 2nd period. During the 3rd period, the potentials become more negative than -350mV. Thus, AE activity during the corrosion process is in good agreement with the decrease trend of the half-cell potentials.

From compatibility between Figure 1 and Figure 14, it is considered that the onset of corrosion in Figure 1 corresponds to the 1st period in Figure 14 and the nucleation of concrete cracking to the 2nd period. Accordingly, at the 1st period, rust layer surface created on rebar could be destroyed.

The corrosion further penetrates inside and at the 2nd period, rust break and other internal cracks inside rebar could occur. At the 3rd period, concrete cracks are nucleated due to expansion of corrosion products in rebar.

5.3 *SEM observation in the accelerated corrosion test*

By SEM (JEOL JSM-5600), observation of rebars was conducted, taking rebar out of the specimen after the 1st period, the 2nd, the 3rd, and at the end. Rust could not be found at the 1st period, while thin rust layer could be identified at the 2nd period by visual observation. The rebar corrosion is distinctively observed at the 3rd period by visual observation. Then, the elements were analyzed by using energy-dispersion typed x-ray spectroscope (EDX). In Figure 15 SEM photos of the end of 1st period are shown. Figure 16 shows the photos of SEM of the end of the 2nd period and Figure 17 shows the photos of SEM of the end of the 3rd period.

At the 1st period in Figure 15, the oxide film at the surface has slightly exfoliated but no corrosion is identified inside. At the 2nd period, the surface oxide film almost exfoliated. As see in Figure 16, the rust on the superficial of a rebar under an oxide film has been identified. With the 3rd period, rust break and other internal cracks inside rebar could occur.

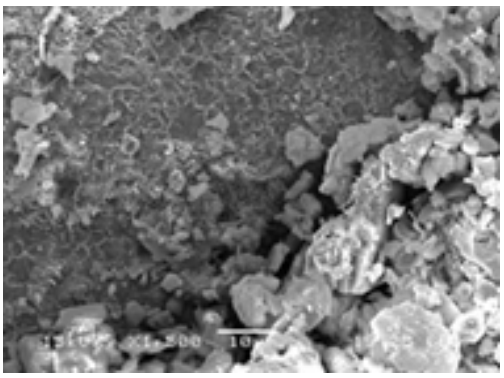

Figure 15.1st period Surface SEM.

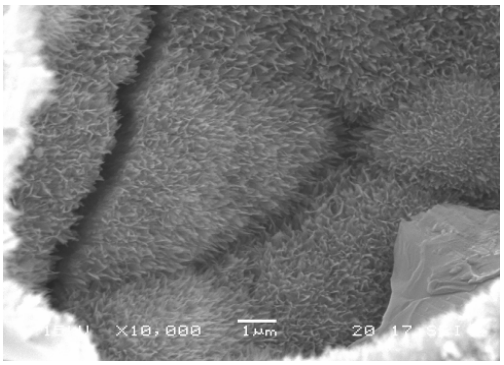

Figure 16.2nd period Surface SEM.

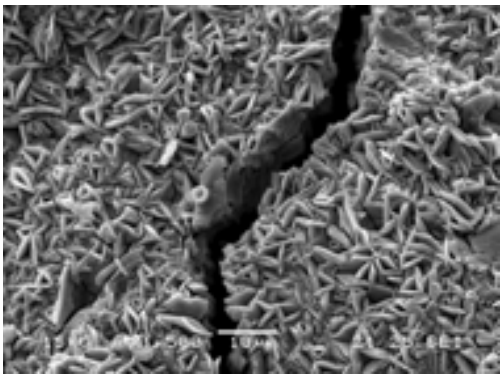

Figure 17.3rd period Surface SEM.

Furthermore, it is identified clearly that the crack inside rebar has occurred at the center. Here, the magnification of the photo of Figure 15 is 1,500. In Figure 16, in contrast, the magnification of a photo is 10,000. Consequently, it is found that expansion pressure is fairly large at the 3rd period. At 1st period, the oxide film on the surface of rebar is broken. At 2nd period, the oxide film was lost, and rust is generated inside rebar. At the 3rd period, the cracks occur inside rebar, and the corrosion becomes accelerated. According to SEM photos, it is realized that at the 1st period, only the surface of rebar is corroded due to permeation of chloride ions. The corrosion penetrates and is nucleated in a whole cross-section at the 3rd period. It is confirmed that the corrosion occurred on the whole rebar surface in the accelerated corrosion test. Further, at the 3rd period, the Cl ion was identified from the surface of a rebar by EDX, suggesting high corrosion rate.

Comparing these SEM photos with AE activity, it is summarized that the 1st period AE activity corresponds to the transition from the dormant stage to the initiation, and the 2nd AE activity is associated with the transition from the initiation to the deterioration. Eventually at the 3rd period AE activity, the acceleration stage starts as active AE generation and rust stain are observed.

5.4 *Results of AE Parameter Analysis*

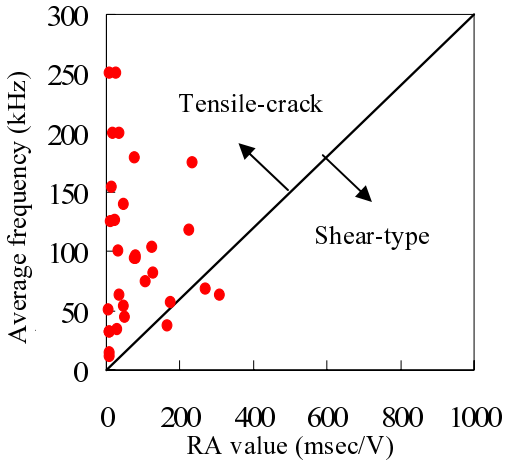

Figure 18. 1st period.

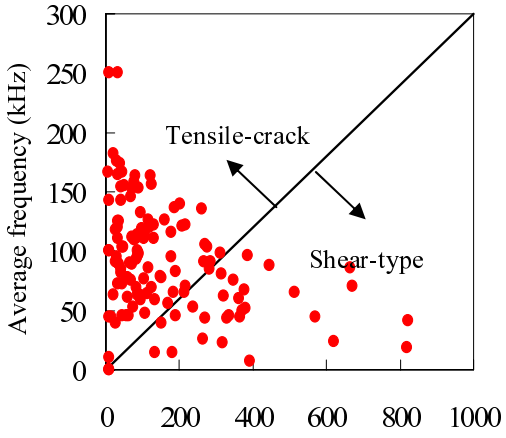

Figure 19. 2nd period.

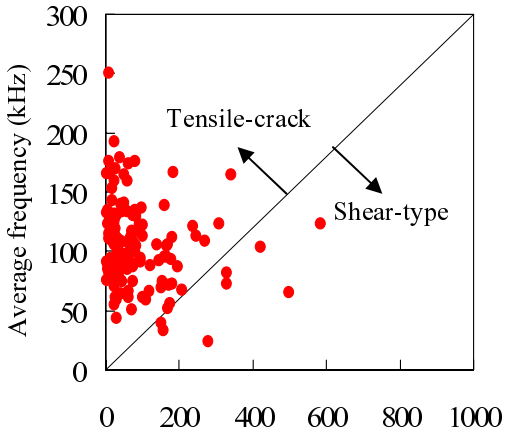

Figure 20. 3rd period.

According to the JCMS-III B5706 standard, a crack type is classified from the relationship between RA value and the average frequency, which is given in Figure 18, Figure 19 and Figure 20. Results of the AE parameter analysis implies that micro-cracks are first accumulated to create the fracture-process zone, and then cracks are visually generated. Furthermore, although tensile cracks are dominantly nucleated at 1st and the 3rd periods, shear-type cracks as well as tensile activity are generated at the 2nd period.

5.5 *Results of SiGMA Analysis*

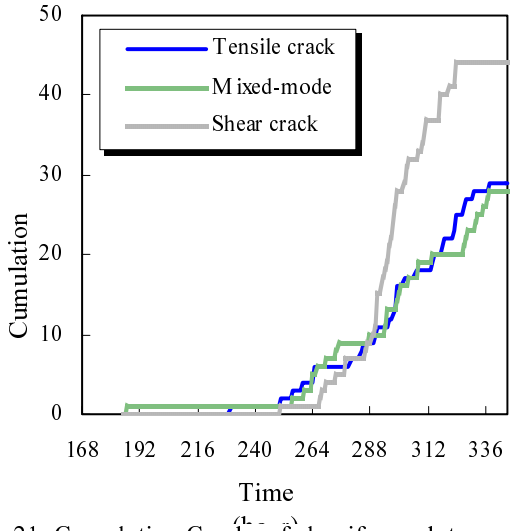

Figure 21. Cumulation Cracks of classify crack type.

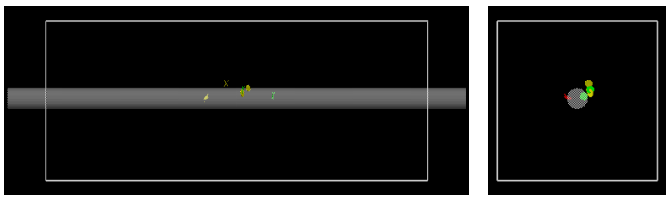

Surface ($x-z$) Surface ($y-z$)

Figure 22. SiGMA analysis (250-263 hours).

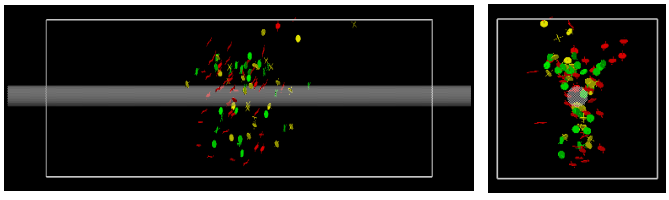

Surface ($x-z$) Surface ($y-z$)

Figure 23. SiGMA analysis (After 250 hours).

It is noted that positions of shear cracks are plotted higher than those of tensile cracks. In the SiGMA analysis, the event definition time (EDT) is set to 30 μsec. EDT uses to recognize waveforms occurring within the specified time from the first-hit waveform and to classify them as part of the current event. Therefore, this time might have influence on AE source locations.

Crack modes of tensile cracks, mixed-mode cracks and shear cracks are given in Figure 21. AE SiGMA analysis during the corrosion process shows in agreement with the increase trend of the tensile cracks and mixed-mode cracks. Later, shear cracks increase more than other cracks. At the initial AE events activities, tensile cracks and mixed-mode cracks increase. After the concrete cracks was observed (229 hours elapsed), generation of shear cracks is confirmed. Accordingly, at the initial concrete cracks, tensile cracks and mixed-mode cracks were generated. Then generation of shear cracks is confirmed.

From 250 hours elapsed to 263 hours, Results of 3-D source location are shown in Figure 22. At the period, internal cracks inside rebar occur were estimated. 3-D source location clearly shows that the crack occurred around rebar. After 250 hours elapsed, results of 3-D source location are shown in Figure 23. Large numbers of micro-cracks are observed around rebar. At this stage, surface cracks were not visually found yet.

6 CONCLUSION

In order to evaluate the deterioration process due to corrosion of reinforced concrete, AE method is applied to the accelerated corrosion test. The following conclusions are obtained.

1 In the accelerated corrosion test, on deterioration process of a RC, the onset of corrosion and the nucleation of concrete cracking are distinguished from AE activity.
2 From SEM, at the 1st period, it is observed that a passive film on the surface of rebar is destroyed. Then, corrosion products on surfaces of rebar grow with time and nucleate micro-cracks in concrete. Further, at the 3rd period, chloride ion penetration accelerates rebar surface corrosion. The corrosion finally is nucleated in a whole cross-section.
3 AE SiGMA analysis during the corrosion process shows in agreement with the increase trend of the tensile cracks and mixed-mode cracks. Later, shear cracks increase more than other cracks.
4 At the initial AE hits activities, internal cracks inside rebar occur were estimated. 3-D source location clearly shows that the crack occurred around rebar. At this stage, surface cracks were not visually found yet. At the final, from rebar to surface are observed.

REFERENCES

ASTM C876. 1991. Standards test method for half-cell potentials of uncoated reinforcing steel in concrete. *Annual book of ASTM standard*.

Dubravka, B. Dunja, M. and Dalibor, S. 2000. Non-Destructive Corrosion Rate Monitoring for Reinforced Concrete Structures. *15th WCNDT*.

Grosse, U. C. Reinhardt, H. and Dahm, T. 1997. Localization and classification of fracture types in concrete with quantitative acoustic emission measurement techniques. *NDT & E International*. Vol.30. No.4: 223-230.

JCMS-III B5706. 2003. Monitoring method for active cracks in concrete by AE. *Japan Construction Material Standards*.

JSCE. 2001. Standerd Specification for Concrete Structures on Maintenance. *Japan Society of Civil Engineers*.

Katsage, T. and Young, R. P. 2007. Acoustic emission and X-ray tomography imaging of shear fracture formation in large reinforced concrete beam. *Proc. of ICAE-6 (CD-ROM)*: 396-401.

Ohtsu, M. 2003. Detection and Identification of Concrete Cracking in Reinforced Concrete by AE. Review of Progress in Quantitative NDE. *AIP conference 2003*. Proc.657. 22B: 1455-1462.

Ohtsu, M. and Tomoda, Y. 2008. Phenomenological model of corrosion process in reinforced concrete identified by acoustic emission. *ACI Materials Journal*, Vol.105. No.2: 194-199.

Ohtsu, M. 1991. Simplified moment tensor analysis and unified decomposition of acoustic emission source : Application to in situ hydrofracturing test. *J. of Geophysical Research*. Vol.96. No.B4: 622-6221.

Ohtsu, M. and Shigeishi, M. Virtual reality presentation of moment tensor analysis by SiGMA. *J. of Korean Soc. for NDT*. Vol.23. No.3: 189-199.

Ohtsu, M. 1996. The history and development of acoustic emission in concrete engineering. *Magazine of Concrete Research*. 48(177): 321-330.

Ohtsu, M. and Ono, K. 1984. A generalized theory of acoustic emission and green's functions in a half space. *J. of Acoustic Emission*. Vol.3. No.1: 124-133.

Ohtsu, M. Okamoto, T. and Yuyama, S. 1998. Moment tensor analysis of acoustic emission for cracking mechanisms in concrete. *ACI Structural Journal*. Vol.95. No.2: pp.87-95.

Ohno, K. Shimozono, S. Sawada. 2008. Y. and Ohtsu, M. Mechanisms of diagonal-shear failure in reinforced concrete beams analyzed by AE-SiGMA. *J. of Solid Mechanics and Materials Engineering*. Vol.2. No.4: 462-472.

Ohno, K. Shimozono, S. Sawada, Y. and Ohtsu, M. 2008. Automatic detection of AE first motion based on AIC picker for SiGMA analysis. *J. of JSNDI*. Vol.57. No.11: 531-536

Yokota, M. 1999. Study on corrosion monitoring of reinforcing steel bars in 36-year-old actual concrete structures. *Concrete library of JSCE*. 33: 155-164.